Int. J. Heat Mass Transfer. Vol. 36, No. 1, pp. 169–175, 1993
Printed in Great Britain

0017-9310/93 $5.00 + 0.00

Boiling heat transfer of a micro-impinging jet of liquid nitrogen in a very slender cryoprobe

TOSHIO AIHARA and JOO-KYUN KIM
Institute of Fluid Science, Tohoku University, Katahira, Aoba-ku, Sendai 980, Japan

and

KAZUYA SUZUKI and KEISUKE KASAHARA
Mayekawa Mfg. Co., Tokyo 135, Japan

(*Received* 13 *January* 1992 *and in final form* 4 *February* 1992)

Abstract—A novel, flexible, long slender cryoprobe with a vacuum insulation layer of outermost diameter 3.1 mm and length 1 m has been developed for cryosurgery of malignancy and cancers. The tip of the cryoprobe was cooled by a micro-impinging jet of liquid nitrogen (LN_2); the maximum cooling heat flux of 1.5 MW m^{-2} was attained. The boiling heat transfer characteristics of the micro-impinging jet were investigated in detail using three types of probe tips: a hemispherical surface and flat surfaces with and without a needle. The effects of the mass flow rate of LN_2, jet mouth-to-tip distance, shape of the probe tip, and surface roughness on boiling heat transfer were examined experimentally. The probe tip with the hemispherical surface finished with a sandpaper of emery No. 500 showed the best cooling performance for cryosurgery.

INTRODUCTION

RECENTLY, a cryosurgical treatment is attracting the attention of clinicians as a cancer-curing method in the medical field. This is a method to remove a malignancy/cancer by freezing rapidly and deeply with a cryogenic stick called a 'cryoprobe' and by necrosing of the target tissue. In general, when spot cooling is applied to a living organ, blood flow onto the spot is increased and the temperature of the target tissue is maintained at the same level as that of the surrounding tissue. Hence, cryosurgery of a living body requires a sufficiently higher cooling rate or higher heat flux than that of dead cellular tissue. Furthermore, the cooling performance of the cryoprobe needs to be controlled dynamically in order to cope with biological reaction and temperature immunity.

Cryoprobes are classified into two types: probes utilizing the Joule–Thomson effect of working gas, and probes using liquid nitrogen (LN_2) [1, 2]. The LN_2 cryoprobe shows excellent cooling performance; in 1964, the first trial probe was developed by Cooper [3] and used for cryosurgical treatment of Parkinson's disease. Since a cryoprobe using cryogenic fluid requires thermal insulation of the entire outside surface of the probe body, except for the probe tip, it was difficult to construct a very slender probe of small diameter and very long length. For example, the probe developed by Cooper and Petrovic [4] had a diameter of 12.7 mm and length of 146.3 mm, and the probe by Augustynowicz and Gage [5] had a diameter of 10 mm and length of 300 mm. Commercial cryoprobes created on the basis of the results of these studies have been used mainly for cryosurgical treatment of cancers formed in locations relatively close to the body surface, as in dermatological and urological diseases [6, 7]. Accordingly, in order to carry out cryosurgical treatment of polyps or cancers formed in the depths of the human body, such as the gullet and stomach, by commercial short probes with a large diameter of 8–20 mm, it is necessary to perform a surgical operation of the abdomen, which results in pain and risk to the patient.

The present authors have developed a cryoprobe with a maximum diameter of 3.1 mm, including an outer insulation layer, and effective length of approximately 1 m. This cryoprobe enables us to perform cryosurgical treatment by inserting it into the channel for vivisectional inspection forceps which is installed within a commercial endoscope. The present report describes the details of this very slender cryoprobe, the experimental results of the cooling performance achieved by boiling heat transfer of a micro-impinging jet of LN_2, and the influence of relevant parameters on the performance.

EXPERIMENTAL APPARATUS AND PROCEDURE

The cross-sectional details of the cryoprobe used in the present experiment are shown in Fig. 1. In order

NOMENCLATURE

A	heat transfer area [m^2]
A_t	cross-sectional area of the cryoprobe tip [m^2]
a	jet mouth-to-tip distance [m]
d_j	jet mouth diameter of inner tube [m]
d_m	diameter of heat transfer surface [m]
$\tilde{h}_v$	latent heat of evaporation [J kg^{-1}]
$\dot{m}$	mass flow rate [kg s^{-1}]
p_j	static pressure at jet mouth [Pa]
Pr	Prandtl number, $\mu c_p/\lambda$
$\dot{Q}$	heat flow rate through the cross-sectional area of probe tip [W]
$\dot{q}$	heat flux at heat transfer surface, $A_t\dot{q}_a/A$ [W m^{-2}]
$\dot{q}_{CHF}$	critical heat flux [W m^{-2}]
$\dot{q}_a$	apparent heat flux per cross-sectional area of probe tip (cooling performance) [W m^{-2}]
$(\dot{q}_a)_{CHF}$	apparent critical heat flux [W m^{-2}]
Re_j	jet Reynolds number, $\rho_j u_j d_j/\mu_j$
T	temperature [K]
T_{sat}	saturation temperature [K]
T_W	inner surface temperature of probe tip [K]
ΔT_{sat}	degree of wall superheat, $T_W - T_{sat}$ [K]
u_j	average jet velocity [m s^{-1}]
x	axial distance from the inner surface toward the heater [m].

Greek symbols

λ	thermal conductivity [W m^{-1} K^{-1}]
μ	absolute viscosity [Pa s]
ρ_l	density of saturated liquid nitrogen [kg m^{-3}]
ρ_v	density of saturated vapor nitrogen [kg m^{-3}]
σ	surface tension [N m^{-1}].

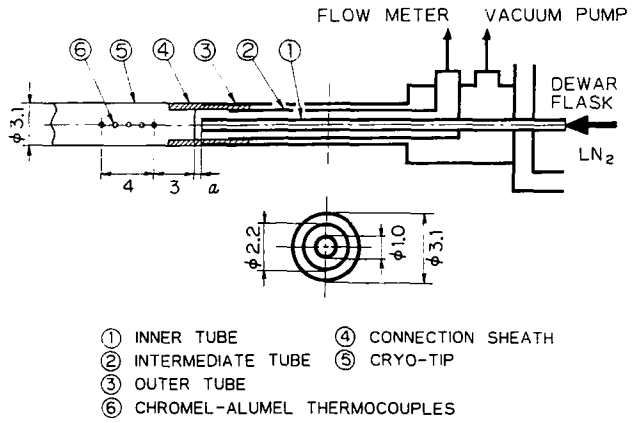

FIG. 1. Cross-sectional details of cryoprobe.

to provide the probe with flexibility and acid resistance, the probe was composed of three gold tubes with different diameters and equal wall thickness of 0.1 mm. The gap space between the outer (3) and intermediate (2) tubes was evacuated to insulate thermally. The outer tube (3) had a diameter of 3.1 mm and a length of 930 mm, the intermediate tube (2) had an outer diameter of 2.2 mm, and the inner tube (1) had an outer diameter of 1.0 mm and length of 1000 mm. Along the central axis of the copper probe tip (5), five 76-μm-diameter chromel–alumel thermocouples (6) were embedded at intervals of 1 mm. As for the inside surface of the probe tip onto which the LN_2 jet impinged, three types, as shown in Fig. 2, were tested: namely, flat surface, hemispherical surface, and flat surface with a needle. The probe tip and body were soft-soldered with a connection sheath (4) to maintain airtightness.

To measure the thermal load of the probe tip, the set-up shown in Fig. 3 was used. The electric input into a 150-W cartridge heater was measured with an ammeter and a digital voltmeter within a measuring

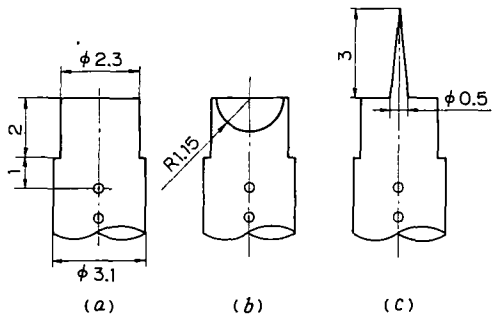

FIG. 2. Cross-sectional view of cryoprobe tips.

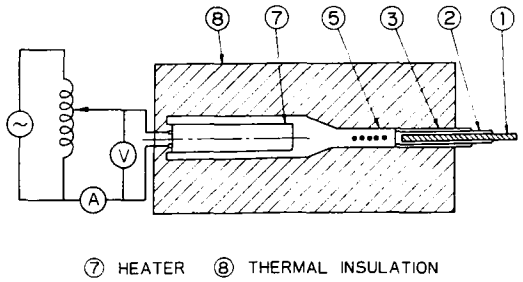

FIG. 3. Details of the measuring section of thermal load.

error of 2.5%. According to a preliminary test, the heat flow rate toward the probe tip through the outer tube was less than 0.5 W.

Figure 4 illustrates an outline of the experimental apparatus and measuring system. LN_2 (9) was pressurized by evaporation within a Dewar vessel (10), allowed to flow out of the exit of the inner tube (1), and then impinged onto the inside surface of the probe tip. After cooling the probe tip, the liquid nitrogen passed through the annular space between the intermediate (2) and inner (1) tubes, and was finally released into ambient air through a thermal mass flowmeter (14) and float-type flowmeter (15). To avoid the formation of a two-phase state in the flowmeters and to maintain a gas temperature between 272 and 313 K, an electric preheater (13) was installed upstream. The values measured from the thermal mass flowmeter were used for data analysis.

The static pressure p_j of the impinging jet was estimated by reducing the contraction and friction losses through the inner tube from the LN_2 pressure of the Dewar vessel. The saturation temperature T_{sat} of LN_2, corresponding to p_j, was determined by a quadratic approximate equation, which was derived from data given in a book [8] of fluid physical properties within an error of $\pm 0.2\%$ in the pressure range of 0.05–0.3 MPa.

The probe tip was cleaned fully with acetone prior to each experiment. The annular insulation layer between the outer (3) and intermediate (2) tubes was evacuated to a vacuum of 10^{-6} Torr by an oil diffusion pump (17) and an oil rotary pump (18).

The axial heat flow rate in the probe tip was determined from the measured temperature gradient and the thermal conductivity of copper, calculated with the cubic approximate equation which was derived from data in the physical property table [9] within an error of $\pm 0.7\%$. Hence, according to error analysis, the maximum error of the temperature gradient in the probe tip is within $\pm 10\%$, that of the temperature T_w is within ± 0.4 K, and the maximum uncertainty in the heat flux in data reduction is within $\pm 11\%$.

RESULTS AND DISCUSSION

Inner surface temperature of the cryoprobe tip

Figure 5 shows a typical axial temperature distribution in the probe tip with a hemispherical surface. It may be seen from the figure that the axial temperature distribution shows excellent linearity. Thus, the inner surface temperature of the probe tip T_w was determined from the linear extrapolation of the measured values by means of the least squares method. The apparent heat flux $\dot{q}_a$ through the probe tip of diameter 3.1 mm was estimated by its temperature gradient and the thermal conductivity of copper at T_w.

Comparison with existing boiling curves

Figure 6 shows a comparison of the present data for LN_2 with steady-state boiling curves previously measured by others, in respect of the heat flux $\dot{q}$ based

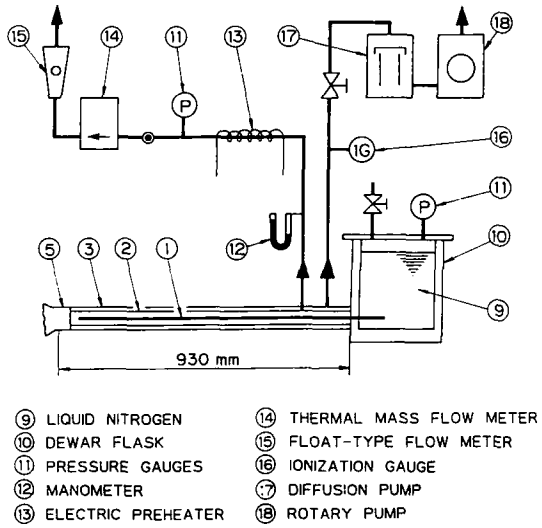

FIG. 4. Outline of experimental apparatus and measuring system.

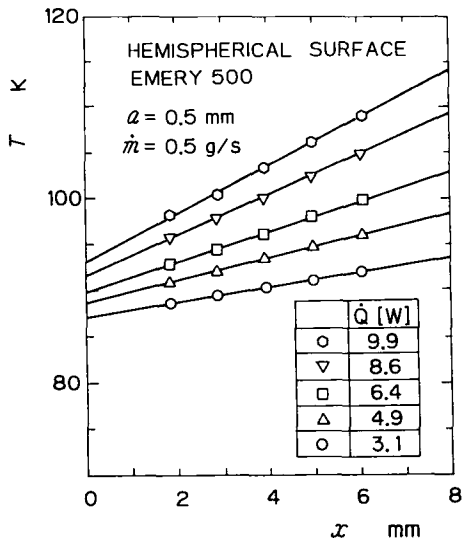

FIG. 5. Typical temperature distributions in a cryoprobe tip.

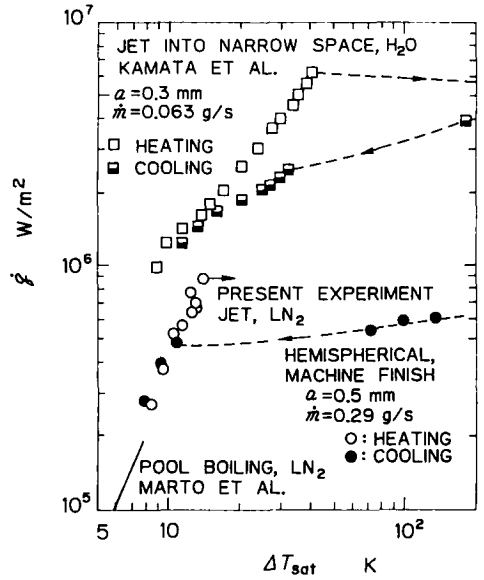

FIG. 6. A comparison of the present data with existing steady-state boiling curves.

on the heat transfer area A. In the figure, the data of Kamata *et al.* [10] are those of boiling heat transfer by an impinging jet of water in a restricted space, and the data of Marto *et al.* [11] are those of nucleate pool boiling of LN_2. The present boiling curve lies between the impinging jet boiling curve for water and the nucleate pool boiling curve for LN_2, and also lies on the extrapolation of the latter. It was also observed in the present experiment that the boiling curve obtained by increasing the heat flux in a quasi-steady state does not coincide with the boiling curve obtained by decreasing the heat flux, and that a hysteresis appears in the boiling curves, as found in conventional pool boiling [12].

From the above comparison, it may be said that the present experiment was conducted with nearly sufficient accuracy. To the authors' knowledge, there are no previous experimental data on impinging jet boiling of LN_2.

Critical heat flux vs average jet velocity

Figure 7 represents a relationship between the critical heat flux based on the heat transfer area, $\dot{q}_{CHF}$, and the average jet velocity, u_j. The value of $\dot{q}_{CHF}$ was determined as the heat flux at the incipience of the rapid increase in ΔT_{sat} under the condition of very gradually increasing heat flux. In the figure, the variation of $\dot{q}_{CHF}$ vs the average jet velocity shows a very similar tendency, regardless of the shape of the heat transfer surface. The difference in $\dot{q}_{CHF}$ between the rough surface finished with emery No. 500 sandpaper and the machine-finished surface is not noticeable. However, $\dot{q}_{CHF}$ for the mirror-finished surface shows a value approximately 12% lower than that of the emery No. 500 sandpaper finish.

The solid line in Fig. 7 represents equation (1), Monde's [13] experimental formula, which was

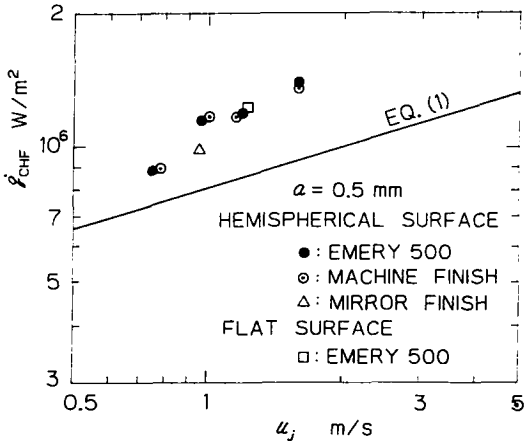

FIG. 7. Relation between critical heat flux and average jet velocity.

derived from data on the critical heat flux for impinging jet boiling of water, R12, and R113 in free space:

$$\frac{\dot{q}_{CHF}}{\rho_v \tilde{h}_v u_j} = 0.211\left(\frac{\rho_l}{\rho_v}\right)^{0.645}\left\{\frac{2\sigma}{\rho_l u_j^2 (d_m - d_j)}\right\}^{0.343} \Big/ \left(1+\frac{d_m}{d_j}\right)^{0.364}. \quad (1)$$

In the figure, the present data on $\dot{q}_{CHF}$ are 20–50% higher than the values evaluated by equation (1). This increase in heat transfer can be attributed to the fact that an impinging jet of LN_2 in an extremely small and confined space produces the returning flow which is effective in separating and removing vapor bubbles from the liquid on the heat transfer surface by centrifugal force.

Influence of the shape of the probe tip

Figure 8 shows the influence of the shape of the inner surface of probe tip on cooling performance,

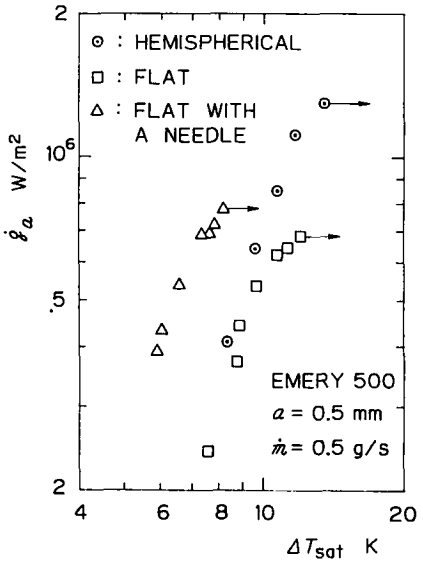

FIG. 8. Influence of the shape of probe tip on apparent heat flux.

exactly defined, the apparent heat flux $\dot{q}_a$ based on the cross-sectional area of the probe tip. In the figure, the arrow-marked data represent those at the critical heat flux.

From the viewpoint of the apparent heat transfer coefficient $\dot{q}_a/\Delta T_{sat}$, the probe tip of the flat surface with a needle shows the best cooling performance because it has a relatively large extended surface for heat transfer and a remarkable forced convection effect in the region of small ΔT_{sat}. However, in the region of high ΔT_{sat} or at the apparent critical heat flux $(\dot{q}_a)_{CHF}$, the probe tip with the hemispherical surface shows the maximum cooling performance. This can be attributed to the following facts. The hemispherical surface has the largest extended heat transfer area, which is almost twice that of the flat surface. In the case of the flat surface with a needle, the flow of LN_2 stagnates at the root of the needle; then, dry spots which are generated in such a stagnation zone are liable to induce burn-out. As a result, the region of nucleate boiling for the hemispherical surface is extended and its critical heat flux is increased to almost twice that for the flat surfaces with/without a needle.

Generally speaking, an increase of several degrees in the tip temperature offers no problems in cryosurgical operation while the maximum apparent heat flux has practical importance. In this sense, the hemispherical surface is the best inner shape for the probe tip.

Influence of the jet mouth-to-probe tip distance

Figure 9 shows the influence of the distance a between the jet mouth and probe tip upon the apparent heat flux q_a. As the distance a is shortened, the apparent heat transfer coefficient $\dot{q}_a/\Delta T_{sat}$ increases and the apparent critical heat flux $(\dot{q}_a)_{CHF}$ becomes high. The reason for this is as follows. Since the present cryoprobe was designed to be a boiling system of the impinging jet in an extremely confined space, a greater distance reduces the impinging rate and velocity (inertia force) of LN_2 onto the heat transfer surface on account of blowing out of nitrogen vapor due to evaporation on the surface and collision with the remaining LN_2 in the turning flow. In the case of a shorter distance, the velocity boundary layer in the wall–jet region, apart from the stagnation point, becomes thinner, and bubbles on the heat transfer surface are effectively removed; consequently, the apparent heat transfer coefficient can be improved.

Figure 10, indicating a correlation between the apparent critical heat flux $(\dot{q}_a)_{CHF}$ and the jet mouth-to-tip distance a, is a more comprehensible explanation of the above-mentioned tendency. It may be seen from the figure that as the distance a is shortened, the apparent critical heat flux increases remarkably.

Influence of the roughness of the heat transfer surface

Figure 11 shows the influence of surface roughness on the apparent heat flux $\dot{q}_a$. In the figure, open circles refer to the rough surface finished with emery No. 500 sandpaper, open squares to the relatively smooth surface by machine-finishing, and open triangles to the mirror-finished surface with a grinding agent after finishing with emery No. 3000 sandpaper. As may be seen from the figure, the rough surface finished with emery No. 500 sandpaper produces the best heat transfer coefficient $\dot{q}_a/\Delta T_{sat}$. Moreover, the apparent critical heat flux of the rough surface is almost the same as that of the machine-finished surface and better than that of the mirror surface. This tendency coincides with the experimental results of pool boiling of Berenson [14] and Marto *et al.* [11].

Influence of mass flow rate

Figure 12 shows the influence of the mass flow rate $\dot{m}$ of LN_2 upon the apparent heat flux $\dot{q}_a$. As the mass

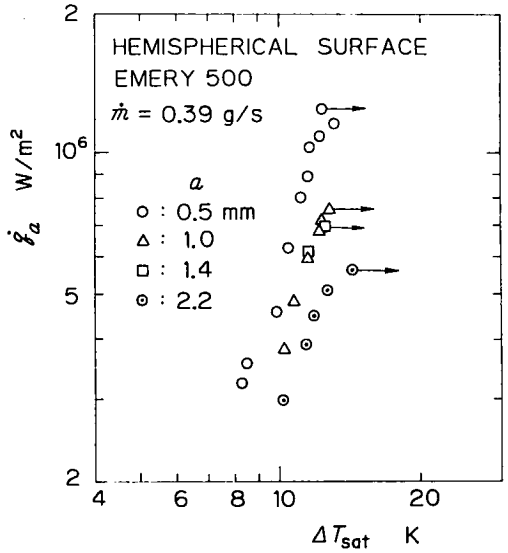

FIG. 9. Influence of jet mouth-to-tip distance.

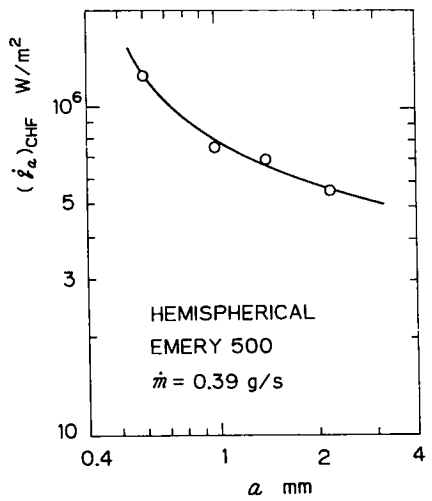

FIG. 10. Relation between the apparent critical heat flux and the jet mouth-to-tip distance.

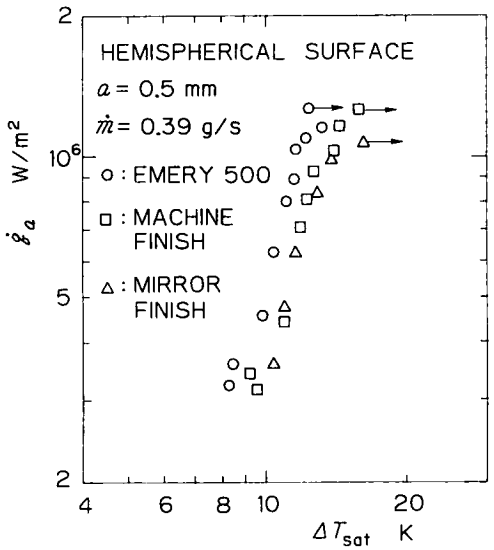

FIG. 11. Influence of surface roughness.

flow rate $\dot{m}$ is increased, the apparent heat transfer coefficient $\dot{q}_a/\Delta T_{sat}$ increases and the apparent critical heat flux $\dot{q}_{CHF}$ also becomes high.

When $\dot{m} = 0.64$ g s^{-1} and $\Delta T_{sat} < 9$ K, the heat transfer phenomenon seems to be in the region of forced convection heat transfer. In the case of Fig. 12, the jet Reynolds number Re_j ($\equiv 4\dot{m}/(\pi d_j \mu)$) is in the range of 3500–8000; consequently, the jet flow can be assumed to be in a turbulent state. Hence, following the established correlation for the heat transfer characteristics of the single-phase impinging jet [15], an empirical equation for the apparent heat flux can be derived from the present experimental data for $\dot{m} = 0.64$ g s^{-1} as

$$\dot{q}_a = 0.253\lambda\, Pr^{0.4}\, Re_j^{0.8}\, \Delta T_{sat}/d_j \qquad (2)$$

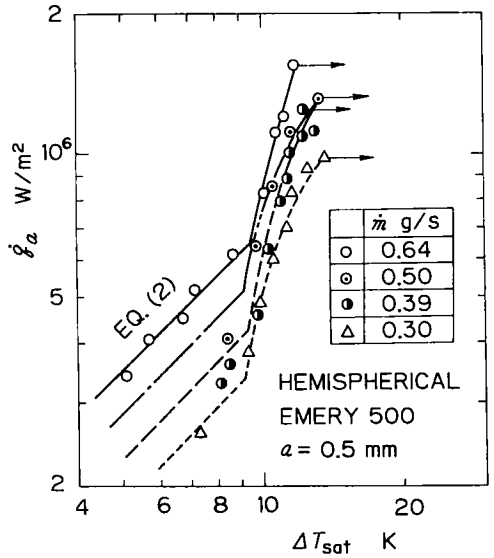

FIG. 12. Influence of jet mass flow rates.

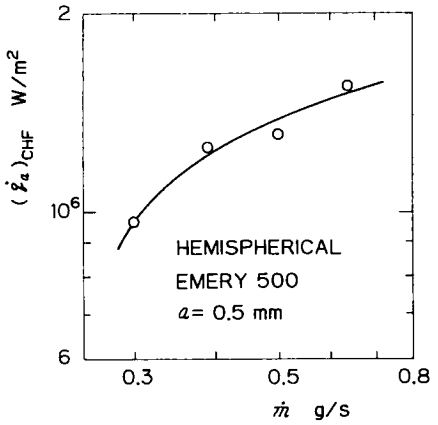

FIG. 13. Relation between the apparent critical heat flux and the mass flow rate.

where physical properties are evaluated at the average temperature $(T_W + T_{sat})/2$. Various straight lines in the region of $\Delta T_{sat} < 9$ K, shown in Fig. 12, are plots of equation (2) for each mass flow rate. The plot of equation (2) for $\dot{m} = 0.3$ g s^{-1} also agrees with the experimental data. From the above investigation, it can be seen that the apparent heat flux is greatly influenced by forced convection when the degree of superheat ΔT_{sat} is small.

Figure 13 shows a correlation between the apparent critical heat flux $(\dot{q}_a)_{CHF}$ and the mass flow rate $\dot{m}$ of the jet. With an increase of the mass flow rate $\dot{m}$ or jet velocity u_j, the contacting time of LN_2 with the heat transfer surface becomes short and the evaporation rate of LN_2 becomes relatively small. Thus, the increasing rate of the apparent critical heat flux $(\dot{q}_a)_{CHF}$ is reduced as $\dot{m}$ is increased. It should be added that the maximum allowable pressure of the Dewar vessel used in the present experiment was 0.2 MPa, the maximum mass flow rate corresponding to this pressure was 0.64 g s^{-1}, and the maximum effective heat flux, or maximum cooling performance, reached approximately 1.5 MW m^{-2}.

CONCLUSIONS

In order to perform cryosurgical treatment by inserting it into the channel for vivisectional inspection forceps which is installed within a commercial endoscope, a very slender cryoprobe with an effective length of approximately 1 m and maximum diameter of 3.1 mm including the outer insulation layer has been developed. The effects of the relevant parameters on boiling heat transfer were studied experimentally. The results obtained are summarized as follows.

(1) The measured critical heat flux, based on the heat transfer area, is 20–25% higher than the value evaluated with Monde's experimental formula, which was derived from the data on impinging jet boiling of water, R12, and R113 in free space, and is little influenced by the roughness of the heat transfer surface.

There is no appreciable difference in the critical heat flux between the flat and hemispherical surfaces.

(2) The probe tip with the hemispherical surface shows the best heat transfer when the degree of wall superheat is greater than 11 K, and its apparent critical heat flux based on the cross-sectional area of the probe tip is almost twice that of the flat surface with or without a needle.

(3) As the distance between the jet mouth and probe tip is increased, the apparent heat transfer coefficient decreases because the impinging velocity of liquid nitrogen onto the heat transfer surface decreases as a result of the blowing out of nitrogen vapor due to evaporation on the surface and collision with the remaining liquid nitrogen in the turning flow.

(4) The influence of surface roughness on the apparent heat flux is similar to a tendency observed in conventional pool boiling, and the apparent heat transfer coefficient of the rough surface finished with emery No. 500 sandpaper is superior to those of machine-finished and mirror-finished surfaces.

(5) As the mass flow rate is increased, the apparent heat transfer coefficient and apparent critical heat flux increase. The apparent heat flux is greatly influenced by forced convection when the degree of wall superheat is below 9 K, and an empirical equation for this region is derived allowing for such experimental facts.

Acknowledgement—This work is part of the research project carried out with a Grant in Aid for Scientific Research B-02555044 from the Ministry of Education, Science and Culture of Japan.

REFERENCES

1. T. Aihara, M. Furukawa and M. Ishimaru, Experimental study on heat-transfer characteristics in a very slender cryoprobe, *Proc. 1st Bioengineering Symp. JSME*, Sendai, pp. 57–58 (1990).
2. T. Aihara, M. Ishimaru and M. Furukawa, Characteristics of heat transfer in a cryoprobe with extremely small diameter, *Proc. 27th Natn. Heat Transfer Symp. of Japan*, Nagoya, Vol. 2, pp. 538–540 (1990).
3. I. S. Cooper, Cryobiology as viewed by the surgeon, *Cryobiology* **1**(1), 44–51 (1964).
4. T. E. Cooper and W. K. Petrovic, An experimental investigation of the temperature field produced by a cryosurgical cannula, *Trans. ASME, J. Heat Transfer* **96,** 415–420 (1974).
5. S. D. Augustynowicz and A. A. Gage, Temperature and cooling rate variations during cryosurgical probe testing, *Int. J. Refrigeration* **8**(4), 198–208 (1985).
6. T. Kamegai and K. Sekiba (Editors), *Cryosurgery*, pp. 52–81. Chugai-Igaku, Tokyo (1976).
7. K. Aso and Y. Sumida, *Low Temperature Medicine*, pp. 304–330. Asakura Shoten, Tokyo (1983).
8. *JSME Data Book: Thermophysical Properties of Fluids*, JSME, Tokyo (1983).
9. Y. S. Touloukian, R. W. Powell, C. Y. Ho and P. G. Klemens, *Thermophysical Properties of Matter*, Vol. 1, pp. 68–81. IFI/Plenum, New York (1970).
10. T. Kamata, S. Kumagai and T. Takeyama, Boiling heat transfer to an impinging jet spurted into a narrow space, *Trans. JSME* **B53**(485), 183–192 (1987).
11. P. J. Marto, J. A. Moulson and M. D. Maynard, Nucleate pool boiling of nitrogen with different surface condition, *Trans. ASME, J. Heat Transfer* **90,** 437–444 (1968).
12. *Boiling Heat Transfer and Cooling*, pp. 12–45. Nihon Kogyo Shuppan, Tokyo (1989).
13. M. Monde, Critical heat flux in saturated forced convection boiling on a heated disk with an impinging jet, *Trans. ASME, J. Heat Transfer* **109,** 991–996 (1987).
14. P. J. Berenson, Experiments on pool-boiling heat transfer, *Int. J. Heat Mass Transfer* **5,** 985–999 (1962).
15. R. J. Goldstein, A. I. Behbahani and K. Heppelmann, Streamwise distribution of recovery factor and the local heat transfer coefficient to an impinging circular air jet, *Int. J. Heat Mass Transfer* **29,** 1227–1235 (1986).